

1 **Inorganic carbon dynamics of melt pond-covered first year sea ice in the**
2 **Canadian Arctic**

3
4 Geilfus N.-X.^{1,2}, Galley R. J.¹, Crabeck O.¹, Papakyriakou T.¹, Landy J.¹, Tison J.-L.³, Rysgaard
5 S.^{1,2,4}

6 ¹ Centre for Earth Observation Science, Department of Environment and Geography,
7 University of Manitoba, Winnipeg, Canada,

8 ² Arctic Research Centre, Aarhus University, Aarhus, Denmark,

9 ³ Laboratoire de Glaciologie, DSTE, Université Libre de Bruxelles, Brussels, Belgium,

10 ⁴ Greenland Climate Research Centre, Greenland Institute of Natural Resources, Nuuk,
11 Greenland.

12

1. Abstract

Melt pond formation is a common feature of spring and summer Arctic sea ice, but the role and impact of sea ice melt and pond formation on both the direction and size of CO₂ flux between air and sea is still unknown. Here we report on the CO₂-carbonate chemistry of melting sea ice, melt ponds and the underlying seawater as well as CO₂ fluxes at the surface of first year landfast sea ice in the Resolute Passage, Nunavut, in June 2012.

Early in the melt season, the increase of the ice temperature and the subsequent decrease of bulk ice salinity promote a strong decrease of the total alkalinity (TA), total dissolved inorganic carbon (TCO₂) and partial pressure of CO₂ (pCO₂) within the bulk sea ice and the brine. As sea ice melt progresses, melt ponds form, mainly from melted snow, leading to a low *in situ* melt pond pCO₂ (36 μatm). The percolation of this low pCO₂ melt water into the sea ice matrix dilutes the brine resulting in a strong decrease of the *in situ* brine pCO₂ (to 20 μatm). This initial low *in situ* pCO₂ observed in brine and melt ponds results in air-ice CO₂ fluxes ranging between -0.04 and -5.4 mmol m⁻² d⁻¹ (negative sign for fluxes out of the atmosphere into the ocean). As melt ponds strive to reach pCO₂ equilibrium with the atmosphere, their *in situ* pCO₂ increases (up to 380 μatm) with time and the percolation of this relatively high concentration pCO₂ melt water increases the *in situ* brine pCO₂ within the sea ice matrix as the melt season progresses. As the melt pond pCO₂ increases, the uptake of atmospheric CO₂ becomes less significant. However, since melt ponds are continuously supplied by melt water their *in situ* pCO₂ still remains undersaturated with respect to the atmosphere, promoting a continuous but moderate uptake of CO₂ (~ -1 mmol m⁻² d⁻¹) into the ocean. Considering the minimum and maximum Arctic sea ice extents during the melt period (90 days), we estimate an uptake of atmospheric CO₂ ranging from 7.3 to 16.4 Tg of C yr⁻¹ due to the sea ice melt pond dynamics. This additional uptake of CO₂ associated to Arctic sea ice needs to be further explored and considered in the estimation of the Arctic Ocean's overall CO₂ budget.

43 2. Introduction

44 The Arctic Ocean represents a global important CO₂ sink, with current estimates of
45 net air to sea CO₂ fluxes between -66 and -199 Tg C yr⁻¹ [Bates and Mathis, 2009;
46 Takahashi et al., 2009]. The role of sea ice in these measured air-sea CO₂ exchanges
47 still remains uncertain [Parmentier et al., 2013] although recent studies suggest that
48 sea ice may act as an important control on the pCO₂ in the ocean surface layer (e.g.
49 Rysgaard et al., [2012b; 2013]). In particular, our understanding of inorganic
50 carbon dynamics during the sea ice melt season and its importance to the annual
51 exchange of CO₂ across the atmosphere-sea ice-ocean interfaces is incomplete. Early
52 studies have suggested that melt ponds could be invoked as significant contributors
53 to the Arctic CO₂ balance through their uptake of CO₂ [Semiletov et al., 2004].
54 However, their impact on inorganic carbon transport through sea ice remains largely
55 uncharacterized, despite the fact that they are a major and increasing surface feature
56 of Arctic sea ice during spring and summer [Rösel and Kaleschke, 2012].

57 Melt ponds cover up to 50-60% of the Arctic summer sea ice area [Fetterer and
58 Untersteiner, 1998; Eicken et al., 2004]. They result from the accumulation of
59 meltwater on sea ice mainly due to melting of snow. Sea ice melt also contributes to
60 the melt pond formation and growth in advanced stages of melt [Rösel and Kaleschke,
61 2012], driven by the increase of short-wave radiation absorption during the summer
62 [Taylor and Feltham, 2004]. During melt pond formation, meltwater either drains
63 into the ocean through cracks and other openings in the sea ice or is collected on the
64 ice surface in depressed areas. This meltwater is nearly free of salt and has a density
65 maximum above the freezing point. Therefore, the radiative heating will favour
66 convection [Fetterer and Untersteiner, 1998]. This convection will be further assisted
67 by winds, increasing temperature erosion of the pond edge eventually extending the
68 pond area. As sea ice warms during spring its brine volume increases and meltwater
69 ponds located above the freeboard may drain by vertical seepage to the underlying
70 water (brine flushing - e.g. Fetterer and Untersteiner [1998]), thereby freshening the
71 upper layer of the ocean. This mechanism is believed to be the primary cause for sea
72 ice desalinisation [Untersteiner, 1968; Cox and Weeks, 1974]. The input of freshwater

73 to the surface layer of the ocean can lead to the formation of under-ice melt ponds,
74 freshwater lenses trapped under thinner ice areas or in depressions in the bottom of
75 thicker ice [Hanson, 1965; Weeks, 2010]. The discharge of melt water through the ice
76 cover is proportional to the ice permeability and the hydraulic pressure gradient in
77 the brine system. In summer Arctic sea ice, this gradient is mostly determined by
78 differences in hydraulic head that develop as a result of melt over a non-uniform ice
79 surface [Eicken et al., 2002].

80 Melt pond formation has a strong impact on the summer energy and mass budgets of
81 an ice cover through the sea ice-albedo-feedback mechanism [Fetterer and
82 Untersteiner, 1998; Taylor and Feltham, 2004; Perovich et al., 2011]. Melt ponds also
83 alter the physical and optical properties of sea ice [Perovich et al., 2002], have a
84 strong influence of the temporal evolution of sea ice salinity [Untersteiner, 1968; Cox
85 and Weeks, 1974] and affect the salt and heat budget of the ocean mixed layer
86 [Eicken et al., 2002; Perovich et al., 2002]. Although a few studies report surface flux
87 measurements of CO₂ during active surface melt [Semiletov et al., 2004; Geilfus et al.,
88 2012b; Nomura et al., 2013], the role of surface melt ponds and the impact of sea ice
89 melt on both the direction and the amount of air-sea CO₂ flux is still not well
90 understood.

91 *Semiletov et al.* [2004], using chambers, documented CO₂ fluxes of -3.9 to -51 mmol
92 m⁻² d⁻¹ (negative flux indicating sea ice uptake of CO₂) across the sea ice-atmosphere
93 interface over melt ponds in June, near to Barrow, Alaska. At that time brine pCO₂
94 was under-saturated (from 220 to 280 μatm) with respect to the atmosphere (365 –
95 375 μatm). This under-saturation was attributed to an increase of photosynthetically
96 active radiation (PAR), which was suggested to have reduced the pCO₂ in the brine
97 by enhancing photosynthesis [Semiletov et al., 2004]. In June 2008, *Geilfus et al.*
98 [2012b] reported CO₂ fluxes over melt ponds and sea ice ranging from -0.02 to -2.7
99 mmol m⁻² d⁻¹, also using the chamber technique over first year sea ice in the Beaufort
100 Sea. These fluxes were substantially smaller than those reported by *Semiletov et al.*
101 [2004], but in the same order of magnitude as those reported during period of melt
102 and surface flooding on Antarctic and Arctic sea ice [Nomura et al., 2013]. In the

103 *Geilfus et al.* [2012b] study, sea ice brine and overlying melt ponds were highly
104 under-saturated in CO₂ relative to atmospheric levels ($p\text{CO}_2$ between 0 and 188 μatm
105 for brine and between 79 and 348 μatm for melt ponds) for the 1.2 m thick landfast
106 sea ice in the Amundsen Gulf (Beaufort Sea). At that time, melt ponds were well
107 established and interconnected. The fresh water originating from internal and
108 surface melting was suggested as an important driver of the observed under-
109 saturation together with other processes, including the dissolution of calcium
110 carbonate and primary production. Using micrometeorological techniques,
111 *Papakyriakou and Miller* [2011] also reported CO₂ uptake with the progression of
112 melt, although flux magnitudes are widely diverging from the chamber-based studies
113 highlighted above.

114 In this study, we examine how the melting of the sea ice cover and the associated
115 formation of melt ponds affects the inorganic carbon dynamic and the air – ice CO₂
116 exchanges. The evolution of the carbonate system was examined using
117 measurements of TA, TCO₂ and $p\text{CO}_2$ on bulk sea ice, brine and melt ponds, in
118 association with CO₂ flux measurements over sea ice and melt ponds. Percolation of
119 melt water from melt ponds was tracked using the isotopic ratios δD and $\delta^{18}\text{O}$ within
120 bulk sea ice and brine.

121 **3. Study site, materials and methods**

122 Field data were collected over first-year landfast sea ice in Resolute Passage,
123 Nunavut, from 3 to 23 June 2012. The sampling site ($\sim 100 \times 100 \text{ m}$) was located
124 between Sheringham Point and Griffith Island (74.726°N, 95.576°W, Figure 1). At the
125 site, adjacent 5 x 5 m areas were chosen for regular sampling for carbonate
126 chemistry determination of ice cores and seawater (on 4-day intervals), while the
127 carbonate chemistry of brine and the surface flux of CO₂ was sampled every 2-days.
128 During our survey, the air temperature increased from 0.6 to 4.3°C (Figure 2).
129 During our first ice station (4 June), coarse wet snow was found at the surface of the
130 ice. On 10 June, the first melt ponds were observed (Figure 2). Once the melt ponds
131 started to form, the ice core and brine sampling was limited to area without melt
132 ponds, referred to as melt hummock.

133 Brine was collected using the sackhole technique (*e.g. Gleitz et al. [1995]*). Sackholes
134 were drilled at incremental depths (20, 40, 75, 100 cm). Brine from adjacent brine
135 channels and pockets was allowed to seep into the sackholes for 5 to 10 min before
136 being collected using a peristaltic pump (Cole Palmer®, Masterflex – Environmental
137 Sampler). Each sackhole was covered with a plastic lid to stop snow falling into the
138 hole.

139 Sea ice core samples were collected using a MARK II coring system (Kovacs
140 Enterprises®). Two ice cores were immediately wrapped in polyethylene (PE) bags
141 and stored horizontally on the sampling site at -20°C in a portable freezer
142 (Whynter® 45 Quart portable Freezer FM-45G) to minimize brine drainage during
143 transport. The first core was dedicated to the analysis of total alkalinity (TA) and
144 total dissolved inorganic carbon (TCO_2). The second core was dedicated to partial
145 pressure of CO_2 in bulk ice (noted as pCO_2 [bulk]) analysis. Two others cores were
146 collected for *in situ* sea ice temperature, bulk ice salinity and ikaite ($CaCO_3 \cdot 6H_2O$)
147 content.

148 Seawater was collected at the ice-water interface through an ice core hole using the
149 peristaltic pump. The same pump was used to collect melt pond samples and an
150 articulated arm was used to collect under-ice melt pond samples. We also collected
151 water column samples at six depths (2, 5, 10, 25, 50, 80 m) using 5 L Niskin bottles
152 for determination of TA and TCO_2 . Vertical profiles of water temperature and salinity
153 were measured with a newly calibrated Sea-Bird SBE 19plus V2 conductivity-
154 temperature depth (CTD) probe.

155 The pCO_2 was measured *in situ* (noted as pCO_2 [*in situ*]) on brine, melt pond water
156 and under-ice seawater using a custom-made equilibration system. The system
157 consists of a membrane contactor equilibrator connected to a non-dispersive
158 infrared gas analyzer (IRGA, Li-Cor 820) via a closed air loop. Brine and airflow rates
159 through the equilibrator and IRGA are approximately 2 l min^{-1} and 3 l min^{-1} ,
160 respectively. Temperature was measured using a calibrated temperature probe
161 (Testo 720®, $\pm 0.1^\circ\text{C}$ precision) simultaneously *in situ* and at the outlet of the

162 equilibrators. Temperature correction of $p\text{CO}_2$ was applied assuming that the relation
163 of *Copin Montégut* [1988] is valid at low temperature and high salinity.

164 Sea ice temperature was measured *in situ* immediately after extraction of the ice
165 cores using a calibrated temperature probe (Testo 720®, $\pm 0.1^\circ\text{C}$ precision) inserted
166 into pre-drilled holes (2.5 cm intervals), perpendicular to core sides. Bulk sea ice
167 salinity and ikaite content was determined on a duplicate ice core sliced into 5 cm
168 sections directly after extraction and placed in sealed containers, which were then
169 placed in a lab fridge to melt at 4°C . These samples were checked regularly, so that
170 the melt water temperature never rose above $1\text{--}2^\circ\text{C}$. Once the samples melted,
171 crystals left in solution were observed on a chilled glass slide under a binocular
172 microscope at room temperature. Finally, the bulk salinity of these samples was
173 measured using a calibrated Thermo-Orion portable salinometer WP-84TPS meter
174 with a precision of ± 0.1 . The sea ice brine volume was calculated according to *Cox*
175 *and Weeks* [1983] for temperatures below -2°C , and according to *Leppäranta and*
176 *Manninen* [1988] between 0°C to -2°C .

177 Samples of melted bulk ice, brine, melt ponds, under-ice melt pond water and
178 underlying seawater were brought back to the University of Manitoba for TA and
179 TCO_2 measurements. Samples were poisoned with a solution of saturated HgCl_2 to
180 prevent any biological activity. The ice core was cut into 10 cm sections in a cold
181 room (-20°C), and each section was placed in a gas-tight laminated (Nylon, ethylene
182 vinyl alcohol, and polyethylene) plastic bag [*Hansen et al.*, 2000] fitted with a 20-cm
183 gas tight Tygon tube and valve. The plastic bag was sealed immediately and excess
184 air was gently removed through the valve using a vacuum pump. The bagged sea ice
185 samples were then melted in the fridge at 4°C and the meltwater mixture and
186 bubbles were transferred to a gas-tight vial (12 ml Exetainer, Labco High Wycombe,
187 UK). TA was determined by potentiometric titration [*Haraldsson et al.*, 1997] with a
188 precision of $\pm 3 \mu\text{mol kg}^{-1}$ while TCO_2 was determined on a TCO_2 auto-analyzer (AS-
189 C3, Apollo SciTech) via sample acidification (H_3PO_4) followed by non-dispersive
190 infrared CO_2 detection (LI-7000) with a precision of $\pm 2 \mu\text{mol kg}^{-1}$. Both TA and TCO_2

191 were calibrated with certified references material from Dr. A. G. Dickson at the
192 Scripps Institution of Oceanography.

193 The ice cores taken for bulk ice $p\text{CO}_2$ analysis were cut into 10 cm sections and
194 stored at -20°C then shipped frozen so that the bulk ice $p\text{CO}_2$ ($p\text{CO}_2[\text{bulk}]$) could be
195 measured at the Laboratoire de Glaciologie, Université Libre de Bruxelles, using the
196 technique developed by *Geilfus et al.* [2012a]. The general principle of the method is
197 to equilibrate the sea ice samples with a mixture of N_2 and CO_2 of known
198 concentration (referred to as the “standard gas”, $146 \mu\text{atm}$) at the *in situ*
199 temperature and rapidly extract the gases into a Varian 3300 gas chromatograph
200 under vacuum. The ice sample is cut to fit tightly the container ($4 \times 4 \times 4.5 \text{ cm}$) to
201 both minimize the headspace volume and keep this headspace constant. The
202 standard gas is injected at 1013 mbar into the container. Then the container with the
203 ice sample is placed in a thermostatic bath setup at the field *in situ* temperature for
204 24 hours. This timing is chosen to ensure that the sample is re-equilibrated to the
205 brine volume and chemical conditions at the *in situ* temperature. A quick injection
206 into the gas chromatograph then allows the reconstruction of the equilibrium brine
207 $p\text{CO}_2$ at the *in situ* temperature. This method is only valid if the ice is permeable at
208 the *in situ* conditions.

209 We determined δD and $\delta^{18}\text{O}$ in 2 ml aliquots of sea ice, brine, under-ice seawater,
210 melt ponds and under-ice melt ponds. Stable isotope measurements were carried out
211 at the University of Manitoba using a Picarro L2130-*i* analyzer. Samples were
212 calibrated against Vienna Standard Mean Ocean Water (VSMOW) with a precision of
213 0.1 ‰ for δD and 0.025 ‰ for $\delta^{18}\text{O}$.

214 CO_2 fluxes at the sea ice surface were measured using a Licor 8100-103 chamber
215 associated with the LI-8100A soil CO_2 flux system. The chamber was connected in a
216 closed loop to the IRGA with an air pump rate at 3 L min^{-1} . $p\text{CO}_2$ in the chamber was
217 recorded every second for 15 minutes and the flux was computed from the slope of
218 the linear regression of $p\text{CO}_2$ against time ($r^2 > 0.99$) according to *Frankignoulle*
219 [1988], taking into account the air volume enclosed within the chamber. The

220 uncertainty of the flux computation due to the standard error on the regression
221 slope was on average $\pm 3\%$.

222 4. Results

223 a. Sea ice

224 The average ice thickness at the sampling site, as determined from cores, decreased
225 from 130 (± 5) to 105 (± 5) cm over the sampling campaign. The mean ice
226 temperature increased from -2.9°C on 4 June to -1.5°C on 12 June (Figure 3). From
227 10 June, the temperature of the top 20 cm of the ice was slightly negative (-0.5°C to
228 0°C) while the rest of the ice thickness remained around -1.5°C . Bulk ice salinity
229 ranged from 7.5 to 0 (Figure 3). The top 20 cm of the ice had salinity around 0 while
230 the bulk salinity of the central part of the ice decreased from 7.5 to 4 during the
231 survey. The salinities associated with the high sea ice temperatures result in brine
232 volumes greater than 5% (data not shown).

233 The $\delta^{18}\text{O}$ and δD isotopic ratios ranged from 1.9 to -23.9‰ and 2.5 to -191.2‰ ,
234 respectively (Figure 3). Profiles of $\delta^{18}\text{O}$ and δD appear to follow the same trend with
235 the lowest values observed in the top 20 cm of the ice cover. Two low events were
236 reported in the upper 20 cm of the ice cover. The first was from 8 to 12 June with an
237 isotopic ratios of $\delta^{18}\text{O}$ and δD as low as -23.9 and -191.2‰ , respectively. The second
238 was on 17 June with $\delta^{18}\text{O}$ and δD of -15.4 and -133.7‰ respectively. The rest of the
239 ice cover ranged from -2 to 1.9‰ for $\delta^{18}\text{O}$ and from -7 to 2.5‰ for δD .

240 The mean total alkalinity in melted bulk sea ice (TA_{ice}) for the entire ice column
241 gradually decreased from $408 \mu\text{mol kg}^{-1}$ on 4 June to $283 \mu\text{mol kg}^{-1}$ on 21 June
242 (Figure 3). This decrease of TA_{ice} was more pronounced in the top 20 cm of the ice
243 cover where the minimal value of $106 \mu\text{mol kg}^{-1}$ was observed on 17 June. The same
244 trend was observed for the total inorganic carbon ($\text{TCO}_{2\text{ice}}$, Figure 3). The mean
245 $\text{TCO}_{2\text{ice}}$ of the entire ice column decreased from $332 \mu\text{mol kg}^{-1}$ on 4 June to $225 \mu\text{mol}$
246 kg^{-1} on 21 June. The minimum values were observed on 17 June, with a mean
247 concentration of $189 \mu\text{mol kg}^{-1}$. To discard concentration – dilution effect, we
248 normalized TA_{ice} and $\text{TCO}_{2\text{ice}}$ to a salinity of 5 (noted as $n\text{TA}_{\text{ice}}$, $n\text{TCO}_{2\text{ice}}$, respectively)

249 because that was the mean bulk salinity of our sea ice samples. The main change
250 observed in normalized values occurred in the top 20 cm. From 4 to 17 June, nTA_{ice}
251 and $nTCO_{2ice}$ increased from 468 and 345 $\mu\text{mol kg}^{-1}$ to 1762 and 1041 $\mu\text{mol kg}^{-1}$
252 while the rest of the ice cover ranged from 337 to 564 $\mu\text{mol kg}^{-1}$ and from 219 to 461
253 $\mu\text{mol kg}^{-1}$, respectively. On 19 and 21 June, in the top 20 cm, nTA_{ice} and $nTCO_{2ice}$
254 decreased to 376 and 323 $\mu\text{mol kg}^{-1}$.

255 From TA_{ice} and TCO_{2ice} , we computed a bulk ice pCO_2 (noted as $pCO_2[\text{bulk_calc}]$)
256 using the CO_2 dissociation constants of *Mehrbach et al.* [1973] refitted by *Dickson*
257 *and Millero* [1987]. This $pCO_2[\text{bulk_calc}]$ ranged from 0 to 32 μatm (Figure 4). On a
258 duplicate ice core, the $pCO_2[\text{bulk}]$ was also measured on solid ice, at the *in situ*
259 temperature, using the sample equilibration technique developed by *Geilfus et al.*
260 [2012a]. The $pCO_2[\text{bulk}]$ ranged from 6 to 182 μatm (Figure 4).

261 We observed few minerals in the ice, which dissolved within a few minutes at room
262 temperature. Due to technical problems we were unable to take any pictures of the
263 crystals. However, as the overall aspect of these crystals look exactly as the crystals
264 found in *Geilfus et al.* [2013a]; [2013b] and [2014] and as they dissolved quickly at
265 room temperature, we assumed they were ikaite (after *Rysgaard et al.* [2012b; 2013;
266 2014]).

267 **b. Brine**

268 From 4 to 10 June, the brine salinity decreased from 55 to 23 (Figure 5). Starting on
269 10 June, low brine salinities (ranging from 1.6 to 11.8) were found at 20 cm depth
270 while deeper brine salinities ranged from 11 to 30, except on 17 June where low
271 salinity were also found at 40 cm depth. The $\delta^{18}O$ and δD isotopic ratios ranged from
272 -1.5 to -15.2‰ and from -15.5 to -118.2‰, respectively (Figure 5). Both profiles
273 appear to be similar, with the lowest values observed at 20 cm depth on 10 June (-
274 15.2‰ and -118.1‰, respectively) and at 20 and 40 cm depth on 17 June (-10.4‰
275 and -87.5‰, respectively).

276 From 4 to 21 June, TA_{br} and TCO_{2br} decreased from their maximum values of 3487
277 and 3189 $\mu\text{mol kg}^{-1}$, to 234 and 270 $\mu\text{mol kg}^{-1}$, respectively (Figure 5). Two periods

278 of low concentrations were observed during our survey. First, on 10 June, minimums
279 of TA_{br} and TCO_{2br} occurred at 20 cm of 501 and 401 $\mu\text{mol kg}^{-1}$ respectively. Then, on
280 17 June, TA_{br} and TCO_{2br} were at 240 and 275 $\mu\text{mol kg}^{-1}$ respectively (at 20 and 40
281 cm). These two minimums in TA_{br} and TCO_{2br} coincided with maximums in nTA_{br} and
282 $nTCO_{2br}$. On 10 June, nTA_{br} and $nTCO_{2br}$ were 596 and 478 $\mu\text{mol kg}^{-1}$, and on 17 June,
283 nTA_{br} and $nTCO_{2br}$ were 874 and 900 $\mu\text{mol kg}^{-1}$.

284 The brine $pCO_2[in situ]$ was under-saturated with respect to the atmosphere (395
285 μatm in June 2012) with values ranging from 20 μatm to 389 μatm (Figure 4, 5).
286 From 4 to 12 June, the mean brine $pCO_2[in situ]$ decreased from 344 to 70 μatm .
287 Then, it increased to 246 μatm on 17 June before decreasing to 81 μatm on 21 June.

288 **c. Melt ponds**

289 On 10 June, melt ponds started to form and were present during the rest of the
290 survey. The melt pond salinity ranged from 1.5 to 2.4 with temperatures from 0°C to
291 0.4°C. The $\delta^{18}O$ and δD isotopic ratios ranged from -3.8 to -10.1‰ and from -40.6 to
292 -93.4‰.

293 TA_{mp} ranged from 219 to 332 $\mu\text{mol kg}^{-1}$ and $TCO_{2 mp}$ ranged from 206 to 306 $\mu\text{mol kg}^{-1}$
294 over the study period. nTA and $nTCO_2$ in the melt ponds ranged from 489 to 972
295 $\mu\text{mol kg}^{-1}$ and 562 to 918 $\mu\text{mol kg}^{-1}$, respectively.

296 Melt pond water was also under-saturated with respect to the atmosphere with a
297 $pCO_2[in situ]$ ranging from 36 to 381 μatm . During the initial formation of melt
298 ponds, their $pCO_2[in situ]$ was low (36 – 84 μatm) but increased to 381 μatm on 17
299 June before fluctuating between 150 and 370 μatm .

300 **d. Underlying seawater**

301 During the survey, the temperature of the seawater layer immediately underlying
302 the sea ice increased from -1.7°C to -1.4°C. The salinity of this layer decreased
303 gradually from 33.2 to 31.4 while the salinity of the water column below 10 m
304 changed much less (Figure 6).

305 The $\delta^{18}\text{O}$ and δD isotopic ratio of the surface layer decreased gradually from their
306 respective maximums of -1.3 and -17.3 ‰ to -2.2 and -19.5 ‰ on 20 June. Deeper
307 layers of the water column ranged from -1.5 and -14.9 ‰ to -1.9 and -18.9‰,
308 respectively (Figure 6).

309 TA_{sw} and $\text{TCO}_{2\text{sw}}$ ranged from 2021 and 1920 $\mu\text{mol kg}^{-1}$ to 2239 and 2167 $\mu\text{mol kg}^{-1}$,
310 respectively. On 20 June, a strong decrease in TA_{sw} and $\text{TCO}_{2\text{sw}}$ was observed, leading
311 to the observed minimum values at the surface of the water column. The normalized
312 TA_{sw} and $\text{TCO}_{2\text{sw}}$ ($n\text{TA}_{\text{sw}}$ and $n\text{TCO}_{2\text{sw}}$ to salinity 5 are shown (Figure 6) to allow
313 direct comparison with the sea ice and brine data) ranged from 319 to 350 $\mu\text{mol kg}^{-1}$
314 and 303 to 333 $\mu\text{mol kg}^{-1}$, respectively.

315 The $p\text{CO}_2[\textit{in situ}]$ of the water column ranged from 259 to 469 μatm . The top 2 m of
316 the seawater column was mainly under-saturated with respect to the atmosphere,
317 except on 7 June where the $p\text{CO}_2[\textit{in situ}]$ was at 455 μatm . From there, the $p\text{CO}_2[\textit{in}$
318 $\textit{situ}]$ decreased to 269 μatm on 23 June (Figure 6).

319 **e. Air – ice CO_2 fluxes**

320 CO_2 fluxes were systematically measured over sea ice and melt ponds (Figure 7)
321 throughout the campaign. Initially, CO_2 fluxes over sea ice were on average at -1.38
322 $\text{mmol m}^{-2} \text{d}^{-1}$. During the initial formation of melt ponds, the fluxes over sea ice
323 peaked at -5.4 $\text{mmol m}^{-2} \text{d}^{-1}$ on 10 June and -2 $\text{mmol m}^{-2} \text{d}^{-1}$ on 12 June. Over melt
324 ponds, the initial uptake of CO_2 was significant at -2.9 $\text{mmol m}^{-2} \text{d}^{-1}$ on 10 June and -
325 4.8 $\text{mmol m}^{-2} \text{d}^{-1}$ on 12 June. Thereafter the uptake of CO_2 by sea ice and melt ponds
326 decreased over time and stabilized at around -1 $\text{mmol m}^{-2} \text{d}^{-1}$.

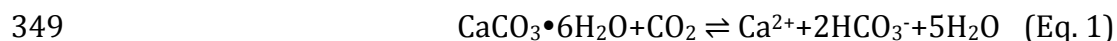
327 **5. Discussion**

328 Over the course of our study period, the vertical temperature gradient within sea ice
329 decreased, leading to a nearly isothermal ice cover. Seasonally rising sea ice
330 temperature was associated with decreasing bulk ice salinity, until ultimately values
331 approached 0 at the surface of the ice cover (Figure 3). The percolation of snowmelt
332 through the ice cover, and its refreezing into the ice matrix formed interposed ice
333 [Landy *et al.*, 2014]. The formation of interposed ice has been described by Freitag

334 *and Eicken [2003] and Polashenski et al. [2012] and could explain the low salinity*
335 *and low $\delta^{18}\text{O}$ and δD isotopic ratio found in the upper 20 cm of the ice cover.*

336 Melt pond formation and subsequent percolation of melt water into the ice cover are
337 visible in the brine system from the isotopic ratio data (Figure 3, 5). The 20 cm depth
338 on 9 and 10 June as well as the 20 and 40 cm depth brine on 17 June had the same
339 isotopic ratios as the melt ponds. The increase of the $\delta^{18}\text{O}$ and δD ratios in the melt
340 ponds observed on 19 and 21 June suggests that the contribution of sea ice melt to
341 the melt ponds had increased. The combination of low $\delta^{18}\text{O}$ and δD values, low bulk
342 salinities (< 5), and warm ice temperatures ($\sim 0^\circ\text{C}$) collectively suggest that melt
343 water percolated into the ice cover, at least to a depth of 40 cm (Figure 5).

344 Previous work has shown brine $p\text{CO}_2$ to change dramatically over the period
345 between sea ice formation and melting [Nomura et al., 2010a; Geilfus et al., 2012b].
346 Increasing ice temperature is associated with decreased brine concentration and
347 brine $p\text{CO}_2$. Brine dilution will also promote the dissolution of ikaite that
348 precipitated in the sea ice, further decreasing the $p\text{CO}_2$ following the reaction:



350 There are several reports of ikaite precipitation in Arctic sea ice [Dieckmann et al.,
351 2010; Rysgaard et al., 2012a; Geilfus et al., 2013a; 2013b; Rysgaard et al., 2013;
352 Sogaard et al., 2013]. In this study however only a few crystals were observed, and
353 they dissolved within minutes after melting the sea ice. Because the overall
354 morphology of these crystals are easily recognized as ikaite and similar to crystals
355 identified as ikaite by x-ray diffraction during other campaigns, we assumed they
356 were ikaite (after [Geilfus et al., 2013a; 2013b; Rysgaard et al., 2013; 2014]). It is not
357 surprising that only small amounts of ikaite crystals were observed in the ice
358 samples as the combination of elevated temperature and brine dilution associated
359 with melting would support the dissolution of ikaite [Rysgaard et al., 2012a].
360 Rysgaard et al. [2014] linked the amount of ikaite content in the ice to the ice
361 temperature, suggesting that as the ice warms up/cooling down, ikaite crystals will
362 dissolve/precipitate. As previously suggested, the dissolution of ikaite crystals

363 during sea ice melt likely contributed to a lowering of *in situ* brine $p\text{CO}_2$ according to
364 equation 1.

365 The concentration of TA and TCO_2 reported in melted bulk sea ice, brine and melt
366 ponds in this study are in the same ranges as those reported from previous studies
367 in the Canadian Archipelago [Rysgaard *et al.*, 2007; Miller *et al.*, 2011; Geilfus *et al.*,
368 2012b; 2013a]. The temperature increase and subsequent salinity decrease promote
369 the overall decrease of TA_{ice} and $\text{TCO}_{2\text{ice}}$ concentrations (Figure 3). The relatively
370 constant $n\text{TA}_{\text{ice}}$ and $n\text{TCO}_{2\text{ice}}$ reported within the ice cover during the survey
371 suggests that the dilution effect was dominant. However, the reduction in TA_{ice} and
372 $\text{TCO}_{2\text{ice}}$ in the top 20 cm of the ice cover was more pronounced after onset of melt
373 pond formation and the formation of interposed ice. These low concentrations are
374 associated with a significant increase of $n\text{TA}_{\text{ice}}$ and $n\text{TCO}_{2\text{ice}}$ during the survey.

375 Decreased brine salinity in response to seasonal warming promoted a decrease in
376 TA_{br} and $\text{TCO}_{2\text{br}}$ [Geilfus *et al.*, 2012b]. The mean TA_{br} and $\text{TCO}_{2\text{br}}$ decreased from
377 3344 and 3037 $\mu\text{mol kg}^{-1}$ on 4 June to 1221 and 1092 $\mu\text{mol kg}^{-1}$ on 10 June, and
378 further to 657 and 579 $\mu\text{mol kg}^{-1}$ on 19 June, with minima observed (i) at 20 cm
379 depth on 10 June, and (ii) at 20 and 40 cm depth on 17 June (Figure 5). Minima in
380 TA_{br} and $\text{TCO}_{2\text{br}}$ were associated with minimum isotopic ratios of $\delta^{18}\text{O}$ and δD , hence
381 we attribute the reduction in carbonate species largely to the percolation of fresh
382 melt water from surface melt ponds into the upper portion of the sea ice volume.
383 $n\text{TA}_{\text{br}}$ and $n\text{TCO}_{2\text{br}}$ remained relatively constant, until the period of melt water
384 percolation, which corresponded to a significant increase in both $n\text{TA}_{\text{br}}$ and $n\text{TCO}_{2\text{br}}$.

385 Melt pond formation and the subsequent percolation of melt water into the ice cover
386 affects TA_{br} and $\text{TCO}_{2\text{br}}$ and appears also affect the *in situ* brine $p\text{CO}_2$ (Figure 5). From
387 4 to 10 June, the decrease of the brine $p\text{CO}_2$ [*in situ*] is mainly due to the drop in brine
388 salinity associated with rising ice temperatures and the dissolution of ikaite. As melt
389 ponds begin to form, their initial $p\text{CO}_2$ is much lower (36 – 84 μatm) than the
390 atmosphere (395 μatm). The percolation of low $p\text{CO}_2$ melt pond water into the ice
391 matrix resulted in a strong decrease in the brine $p\text{CO}_2$ [*in situ*] observed at 20 cm
392 depth on 9 and 10 June. However, over time, the melt pond $p\text{CO}_2$ [*in situ*] increased

393 as it equilibrated with the atmosphere (Figure 5). The subsequent percolation of this
394 higher $p\text{CO}_2$ melt water into the ice matrix resulted in an increase in brine $p\text{CO}_2$
395 within the sea ice observed on 17 June. The melt pond $p\text{CO}_2$ [*in situ*] decreased
396 slightly (150 μatm on 19 June) as did the brine $p\text{CO}_2$ (to <100 μatm) as a result of
397 melt water being added to the pond. By 21 June, the $p\text{CO}_2$ in the melt pond had
398 increased as a result of CO_2 uptake from the atmosphere.

399 The sea ice $p\text{CO}_2$ [bulk] measured on solid ice samples (Figure 4) are in the same
400 range as those reported by *Geilfus et al.* [2012a] on landfast sea ice sampled during
401 the same season in Barrow, Alaska. The ice characteristics were similar to our
402 survey; a nearly isothermal ice cover (approaching 0°C), low salinity in the surface
403 layer (0-20 cm) and melt ponds at the surface of the ice [*Zhou et al.*, 2013]. *Crabeck*
404 *et al.* [2014] also reported sea ice $p\text{CO}_2$ [bulk] from SW Greenland. However, the
405 concentrations reported in our study are in the lower end compared with the
406 concentrations of 77-330 μatm reported by *Crabeck et al.* [2014]. The lower
407 concentrations during our study may be due to warmer sea ice leading to a lower
408 $p\text{CO}_2$ due to brine dilution by fresh melt water and/or dissolution of ikaite. These
409 concentrations can be compared with the $p\text{CO}_2$ [bulk_calc] (Figure 4). However, the
410 $p\text{CO}_2$ [bulk_calc] rely on the validity of the four equilibrium constants of the aqueous
411 carbonate system. The thermodynamic constants are assumed to be valid at subzero
412 temperatures, but this assumption needs to be tested. Moreover, the $p\text{CO}_2$ [bulk_calc]
413 is not representative of the *in situ* concentrations because the ice sample is melted.
414 Melt will trigger the dissolution of ikaite crystals that may have formed, strongly
415 impacting both the TA and the $T\text{CO}_2$ of the resulting meltwater. On the contrary, the
416 ice $p\text{CO}_2$ [bulk] measured the CO_2 concentration at the *in situ* temperature, so it takes
417 into account the CO_2 dissolved within the brine as well as the gaseous CO_2 (bubbles)
418 in the ice sample. The range of $p\text{CO}_2$ [bulk_calc] is in the lower end of $p\text{CO}_2$ [bulk].
419 However, both calculated and measured bulk $p\text{CO}_2$ show an over-all drop in $p\text{CO}_2$
420 associated with brine dilution and the dissolution of ikaite. While the ice
421 $p\text{CO}_2$ [bulk_calc] only shows a slight decrease over time, the ice $p\text{CO}_2$ [bulk] reveals
422 that larger changes may occur, especially in the upper 20 cm of the ice cover (Figure

423 4). The ice $p\text{CO}_2[\text{bulk}]$ and brine $p\text{CO}_2[\text{in situ}]$ differ in that a significant decrease of
424 the brine $p\text{CO}_2[\text{in situ}]$ was observed on 12 June, just after melt pond formation,
425 whereas only a slight decrease was observed in the ice $p\text{CO}_2[\text{bulk}]$ time series. The
426 percolation of melt water with low *in situ* $p\text{CO}_2$ initiated a drop in the brine $p\text{CO}_2[\text{in}$
427 *situ}] to similar concentrations as in the melt ponds. Other examples are observed on
428 17 June, then again on 19 and 21 June. On 17 June, high *in situ* $p\text{CO}_2$ melt water
429 percolation through the ice matrix was associated with an increase in brine $p\text{CO}_2[\text{in}$
430 *situ}] whereas the ice $p\text{CO}_2[\text{bulk}]$ remained constant. On 19 and 21 June, the brine
431 $p\text{CO}_2[\text{in situ}]$ decreased to reach the same concentration as the ice $p\text{CO}_2[\text{bulk}]$.**

432 To test the sackhole technique's ability to sample uncontaminated brine, we
433 compared TA_{br} and $\text{TCO}_{2\text{br}}$ with a TA and TCO_2 estimated from TA_{ice} and $\text{TCO}_{2\text{ice}}$ and
434 the calculated brine volume (Figure 8) [Cox and Weeks, 1983; Leppäranta and
435 Manninen, 1988]. Both methods yield similar TA and TCO_2 concentrations (from 274
436 to 3554 $\mu\text{mol kg}^{-1}$ and from 283 to 3189 $\mu\text{mol kg}^{-1}$, respectively), with a similar
437 relationship between TA and TCO_2 with a R^2 's of 0.84 and 0.85, respectively. The
438 scatter between the two methods could be due to the impossibility of determining
439 the exact original depth from which the brine seeped, especially if melt ponds are
440 present at the surface of the ice cover.

441 As melt ponds developed, freshwater percolated through the ice matrix and could
442 form a freshwater layer beneath the sea ice [Hanson, 1965]. An accumulation of
443 under-ice melt water was not observed during our survey. Perhaps this is because
444 the stage of ice melt was not sufficiently advanced and/or under-ice currents
445 effectively mixed the freshwater layer beneath the ice. The only noticeable impact of
446 the percolation of melt ponds water on the underlying seawater was observed on 20
447 June where the decrease of TA_{sw} and $\text{TCO}_{2\text{sw}}$ was associated with the low isotopic
448 ratio of $\delta^{18}\text{O}$ and δD captured over a very short period (Figure 6).

449 As in previous studies, the relationships between $n\text{TA}$ and $n\text{TCO}_2$ in seawater, brine
450 and sea ice samples can be use to determine the main processes affecting the
451 carbonate system. In Figure 9, the dotted lines represent the response of inorganic
452 carbon and alkalinity to different processes (after Zeebe and Wolf-Gladrow [2001]).

453 An exchange of $\text{CO}_{2(\text{gas})}$ will affect TCO_2 while TA will remain constant. The
454 precipitation – dissolution of ikaite will affect TA and TCO_2 in a ratio of 2:1. Biological
455 activity will increase TA slightly and reduce TCO_2 slightly in the ratio $\text{TA}:\text{TCO}_2 = -$
456 0.16 [Lazar and Loya, 1991]. To calculate these theoretical effects we assumed that
457 seawater sampled at 50 m (on average: $T = -1.62^\circ\text{C}$; $S = 32.43$; $\text{TA} = 2229 \mu\text{mol kg}^{-1}$
458 and $\text{TCO}_2 = 2135 \mu\text{mol kg}^{-1}$, Figure 6) was not influenced by the overlying melting
459 sea ice. $n\text{TA}$ and $n\text{TCO}_2$ data from sea ice samples are located along the ikaite
460 dissolution line while brine and melt pond samples are located between the ikaite
461 dissolution line and the CO_2 uptake line, suggesting both processes occurred in
462 combination. We posit that ikaite crystals formed in winter were dissolved during
463 spring, thereby lowering $p\text{CO}_2$ and enhancing CO_2 uptake. The dissolution of the
464 ikaite crystals will increase $n\text{TA}$ and $n\text{TCO}_2$ (in a ratio 2:1) in the upper brine layer
465 and melt pond while the uptake of CO_2 will only increase $n\text{TCO}_2$. This explains the
466 high $n\text{TA}$ and $n\text{TCO}_2$ reported in the Figure 5. It is lent further credibility by the small
467 amount of ikaite crystals observed in the sea ice. The mean concentration of algal
468 biomass (Chl *a*) in bulk sea ice decreased from decreased from $23.15 \mu\text{g L}^{-1}$ in 4 June
469 to $1.11 \mu\text{g L}^{-1}$ on 12 June and Chl *a* concentration in melt ponds ranged from 0.08 to
470 $0.41 \mu\text{g L}^{-1}$ (unpublished data, C. Mundy and V. Galindo). The loss of the biomass
471 could result from the warming and melting of the ice [Zeebe *et al.*, 1996; Galindo *et*
472 *al.*, 2014]. These concentrations are in the same range as those reported by Mundy *et*
473 *al.* [2011] and Geilfus *et al.* [2012b] on melting landfast sea ice in the Beaufort Sea.
474 From the brine profiles in Figure 5 and from the trend of the sea ice samples in
475 Figure 9, it looks like brine dilution and calcium carbonate dissolution are the main
476 factors controlling CO_2 exchange during our observation period. It should however
477 be underlined that most of the calcium carbonate dissolution trend holds in only 4-5
478 samples located in the top 20 cm of the sea ice cover. In the lowest range of $n\text{TA}$ and
479 $n\text{TCO}_2$ ($< 500 \mu\text{mol kg}^{-1}$) which correspond to 80% of the sea ice cover (including the
480 bottom Chl *a* rich 10 cm layer), the ice samples pull the trend to the left of the
481 calcium carbonate dissolution line, suggesting an increasing influence of the algal
482 CO_2 uptakes, strong enough to maintain the bottom ice and brines $p\text{CO}_2$ at low
483 values, in the close vicinity of the nearly saturated water values at the ice-water

484 interface. This biological effect on the TCO_2 is however probably limited to the
485 decaying very bottom section of the sea ice cover [Søgaard *et al.*, 2013; Glud *et al.*,
486 2014]. This is similar to what has been described in the Beaufort Sea (Arctic, Geilfus
487 *et al.* [2012b]) and in the Weddell Sea (Antarctica, Papadimitriou *et al.* [2012]) on
488 landfast sea ice, although during early spring, i.e. at ice temperatures colder than
489 those observed during the present study. Therefore sea ice and brine samples from
490 these other studies are located on the other side of the seawater value, i.e. lying
491 between the precipitation of calcium carbonate and the release of CO_2 , in the
492 $nTA/nTCO_2$ space.

493 The CO_2 fluxes reported here are lower than fluxes reported by Semiletov *et al.*
494 [2004] over melt ponds, but similar to fluxes reported by Geilfus *et al.* [2012b] over
495 sea ice and melt ponds and similar to fluxes reported by Nomura *et al.* [2013] on
496 Antarctic and Arctic sea ice during periods of snowmelt and surface flooding. CO_2
497 fluxes over sea ice depend on the ice permeability and the CO_2 concentration
498 gradient between the ice surface and the atmosphere conveyed through the liquid
499 phase (*i.e.* brine and melt water). Brine and melt ponds were under-saturated with
500 respect to the atmosphere (Figure 5). The sea ice uptake of atmospheric CO_2 was at
501 first moderate ($\sim -1 \text{ mmol m}^{-2} \text{ d}^{-1}$, Figure 7) due to brine being slightly under-
502 saturated. Then the decrease of the brine $pCO_2[in situ]$ due to the percolation of melt
503 water with low *in situ* pCO_2 intensified the uptake of atmospheric CO_2 (up to -5.4
504 $\text{mmol m}^{-2} \text{ d}^{-1}$) by the ice. As the brine $pCO_2[in situ]$ increased, the uptake of CO_2
505 decreased accordingly ($\sim -1 \text{ mmol m}^{-2} \text{ d}^{-1}$). In addition, insignificant fluxes (in the
506 range of $-0.005 \text{ mmol m}^{-2} \text{ d}^{-1}$) were detected over interposed ice, as Nomura *et al.*
507 [2010b] and Geilfus *et al.* [2012b] who reported fluxes $\sim 0 \text{ mmol m}^{-2} \text{ d}^{-1}$ on
508 superimposed ice. During the initial formation of melt ponds, the low *in situ* pCO_2
509 promoted a strong uptake of atmospheric CO_2 ($-3.8 \text{ mmol m}^{-2} \text{ d}^{-1}$). However, as the
510 melt pond $pCO_2[in situ]$ approached equilibrium with the atmosphere, their CO_2
511 uptake decreased and stabilized around $\sim -1 \text{ mmol m}^{-2} \text{ d}^{-1}$.

512 To estimate a total uptake of atmospheric CO_2 (Figure 7) over the sampling area (F_{tot} ,
513 crosses), we used the pond coverage (fraction $0 \leq x \leq 1$) (Figure 2) to weight the

514 fluxes over sea ice (F_{ice} , open circles) and over melt ponds (F_{mp} , black triangles),
515 respectively, using the following equation:

$$F_{tot} = F_{ice} \cdot (1 - x) + F_{mp} \cdot x$$

516 The pond coverage (Figure 2) was obtained six times between the date of pond onset
517 (10 June) and the final sampling date with a terrestrial laser scanner. The scanner
518 was used to measure the surface topography of an untouched 80 x 160 m area of sea
519 ice and could differentiate between ice cover and melt ponds at the surface,
520 providing the pond fraction [Landy *et al.*, 2014]. F_{tot} peaked during the initial
521 formation of the melt ponds, then returned to previous values ($-1 \text{ mmol m}^{-2} \text{ d}^{-1}$)
522 when melt ponds were the dominant surface feature. $p\text{CO}_2$ conditions in melt ponds
523 are determined by a balance between equilibration with atmospheric CO_2 and the
524 continuous supply of low- $p\text{CO}_2$ melt water from melting snow and sea ice. This
525 allows melt ponds to be a continuous but moderate CO_2 sink. Therefore, if we take
526 into account a mean uptake of CO_2 of $-1 \text{ mmol m}^{-2} \text{ d}^{-1}$, over the minimum and
527 maximum Arctic sea ice extent during spring and summer thaw (90 days), we derive
528 an uptake from 7.3 to 16.4 Tg of C yr^{-1} . However, mixing the melt of the sea ice
529 observed during this study (with average characteristics of $T = -1.1 \text{ }^\circ\text{C}$, $S = 3.8$, $\text{TA} =$
530 $296 \text{ } \mu\text{mol kg}^{-1}$ and $\text{TCO}_2 = 228 \text{ } \mu\text{mol kg}^{-1}$) in a 20 m thick mixed layer (with average
531 water column characteristics of $T = -1.62^\circ\text{C}$; $S = 32.43$; $\text{TA} = 2229 \text{ } \mu\text{mol kg}^{-1}$ and TCO_2
532 $= 2135 \text{ } \mu\text{mol kg}^{-1}$), will result in a 9.4 ppm decrease in the seawater composition and
533 an oceanic uptake of $0.55 \text{ mmol of } \text{CO}_2 \text{ m}^{-2} \text{ d}^{-1}$ over the 90 days of spring and summer
534 thaw. This corresponds to a total oceanic uptake of 4.97 Tg of C yr^{-1} . Rysgaard *et al.*
535 [2011] estimated an overall budget for the Arctic sea ice between 14 and 31 Tg of C
536 yr^{-1} depending on whether the precipitation of calcium carbonate took place in the
537 ice or not. Other estimates of carbon uptake by the Arctic Ocean include Takahashi *et*
538 *al.* [2009], who estimated an uptake of 121 Tg of C yr^{-1} for an area north of 66°N
539 while Bates and Mathis [2009] estimated an uptake between 66 and 199 Tg of C yr^{-1}
540 for the Arctic Ocean. However, these works ignored the role of the Arctic sea ice and
541 considered it an impermeable barrier, impeding the gas exchanges between the
542 ocean and the atmosphere. We have shown things may be more complicated and in

543 fact sea ice may play an important role in mediating the exchange of CO₂ between the
544 atmosphere and ocean at high latitudes.

545 **6. Conclusions**

546 We investigated the evolution of inorganic carbon within landfast first-year sea ice in
547 Resolute Passage, Nunavut, from 3 to 23 June 2012 during the spring and summer
548 melt period. Temperature profiles became isothermal ($\sim -1^{\circ}\text{C}$) with low salinity at
549 the surface (~ 0). Melt ponds started to form at the surface of the ice on 10 June.

550 Early in the melt period, increased ice temperatures and subsequent decreased bulk
551 ice salinity and dissolution of ikaite crystals promoted a strong decrease of TA, TCO_2
552 and pCO_2 observed in bulk sea ice and brines (Figure 10a). The decrease of pCO_2
553 caused sea ice to act as a sink for the atmospheric CO₂ ($\sim -1 \text{ mmol m}^{-2} \text{ d}^{-1}$). This sink
554 increased (up to $-5.4 \text{ mmol m}^{-2} \text{ d}^{-1}$) during the initial formation of melt ponds due to
555 their very low pCO_2 levels. The percolation of melt pond water into the ice matrix
556 increased brine dilution and decreased brine TA, TCO_2 and pCO_2 (Figure 10b). Low
557 TA_{br} and TCO_{2br} concentrations observed were associated with the percolation of
558 melt water from melt ponds, and the brine $pCO_2[in situ]$ was controlled by the melt
559 ponds. As melt ponds formed from melted snow and surface sea ice melt, the melt
560 pond $pCO_2[in situ]$ was low ($36 \mu\text{atm}$). The percolation of this low pCO_2 , low salinity
561 melt water into the sea ice matrix decreased the brine $pCO_2[in situ]$ to $20 \mu\text{atm}$. As
562 sea ice temperatures rose, melt water was continuously supplied to the ponds, which
563 prevented melt ponds from fully equilibrating with the atmospheric CO₂. Instead,
564 pCO_2 in the melt ponds fluctuated between $0 \mu\text{atm}$ and the atmospheric
565 concentration ($395 \mu\text{atm}$). As melt ponds reached equilibrium with the atmosphere,
566 their uptake became less significant. But as melt ponds are continuously supplied
567 with fresh melt water while simultaneously draining to the ocean, the melt pond
568 $pCO_2[in situ]$ remained under-saturated and promoted a continuous but moderate
569 uptake of CO₂ from the atmosphere ($\sim -1 \text{ mmol m}^{-2} \text{ d}^{-1}$).

570 Based on the present study, we estimate the CO₂ flux due to melt ponds in the Arctic
571 to be in the order of -7.3 to $-16.4 \text{ Tg of C yr}^{-1}$. This is a 5 – 15 % addition to the total

572 uptake for the Arctic Ocean previously reported when sea ice was considered a
573 barrier to these fluxes [*Bates and Mathis, 2009; Takahashi et al., 2009*].

574 **7. Acknowledgments**

575 This study was funded by the Canada Excellence Research Chair (CERC, S.R.), the
576 Natural Sciences and Engineering Research Council (NSERC) of Canada (T.P.) and
577 from the Bigsouth Belspo project (J.-L. T.) # SD/CA/05A . This work is a contribution
578 to the Arctic Science Partnership (ASP), the ArcticNet Networks of Centres of
579 Excellence programs and the SCOR BEPSII project. The authors are grateful to the
580 anonymous reviewers whose comments greatly improved the quality of the
581 manuscript.

582

583

584 8. Figure captions

585 Figure 1: Location map of the sampling area in the Resolute Passage, Nunavut. The
586 sampling site was located between Sheringham Point and Griffith Island
587 (74.726°N, 95.576°W).

588 Figure 2: (a.) Evolution of the atmospheric temperature in Resolute from the end of
589 May to the end of June 2012. The black dots represent the air temperature
590 during our survey (from 3 to 23 June). (b.) Evolution of the melt ponds
591 (black dots) and sea ice (white dots) fraction coverage at the sampling site.
592 The bold dashed line on 10 June represents the initial formation of melt
593 ponds at the surface of the ice cover. Aerial photo were taken over the field
594 study site on 13 June (pond fraction = 0.9; width of the picture = 4472m),
595 23 June (pond fraction = 0.65; width of the picture = 2212m), 29 June
596 (pond fraction = 0.61; width of the picture = 4426m).

597 Figure 3: Sea ice profiles of temperature (°C), salinity, isotopic composition of $\delta^{18}\text{O}$
598 and δD (‰), TA_{ice} and $n\text{TA}_{\text{ice}}$ (in $\mu\text{mol kg}^{-1}$), TCO_2 and $n\text{TCO}_{2\text{ice}}$ (in $\mu\text{mol kg}^{-1}$).
599

600 Figure 4: Sea ice profiles of $p\text{CO}_2$ (μatm) calculated from TA_{ice} and $\text{TCO}_{2\text{ice}}$ (grey
601 diamonds) and *in situ* bulk sea ice $p\text{CO}_2$ (white diamonds). The *in situ* brine
602 and melt ponds $p\text{CO}_2$ are also represented (back dots and triangle,
603 respectively).

604 Figure 5: Profiles of *in situ* brine $p\text{CO}_2$ (in μatm), salinity, isotopic composition of $\delta^{18}\text{O}$
605 and δD (‰), TA_{br} and $n\text{TA}_{\text{br}}$ (in $\mu\text{mol kg}^{-1}$), $\text{TCO}_{2\text{br}}$ and $n\text{TCO}_{2\text{br}}$ (in $\mu\text{mol kg}^{-1}$).
606

607 Figure 6: Water column profiles of temperature (°C), salinity, isotopic composition of
608 $\delta^{18}\text{O}$ and δD (‰), TA and $n\text{TA}$ (in $\mu\text{mol kg}^{-1}$), TCO_2 and $n\text{TCO}_2$ (in $\mu\text{mol kg}^{-1}$)
609 and calculated $p\text{CO}_2$ (in μatm).

610 Figure 7: CO_2 fluxes (in $\text{mmol m}^{-2} \text{d}^{-1}$) measured over sea ice (white diamonds), melt
611 ponds (black triangle). The total fluxes are represented by the black cross.

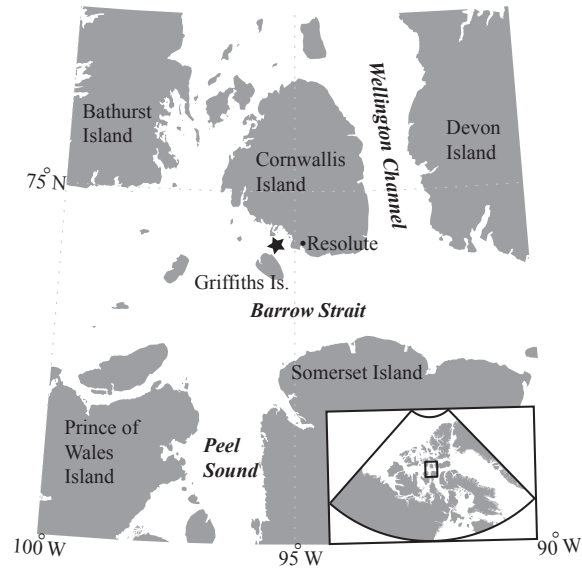
612 Figure 8: Comparison between brine TA and TCO_2 measured on brine collected using
613 the sackholes technique and the brine TA and TCO_2 estimated from TA_{ice} ,
614 TCO_{2ice} and the brine volume.

615 Figure 9: Relationship between the $nTCO_2$ and nTA (in $\mu\text{mol kg}^{-1}$) in bulk sea ice
616 (white diamonds), melt ponds (grey triangle) and brine samples (black
617 dots). The different dashed lines represent the theoretical evolution of
618 $nTA:nTCO_2$ ratio following the precipitation/dissolution of calcium
619 carbonate, release/uptake of $CO_{2(g)}$ and biological
620 photosynthesis/respiration.

621 Figure 10: Schematic illustration of the inorganic carbon dynamics of melt pond-
622 covered first year sea ice. (a.) The increase of the ice temperature and the
623 decrease of the salinity, associated with the dissolution of ikaite crystals
624 promote the decrease of the bulk ice and brine pCO_2 . (b.) Formation of melt
625 ponds at the surface of the ice and percolation of meltwater into the ice
626 matrix further decreases the pCO_2 with episodes of partial recovery, due to
627 surface exchanges with the atmosphere. The pCO_2 level is indicated by the
628 size of the writing. The intensity of the CO_2 uptake is indicated by the size
629 of the arrow.

630

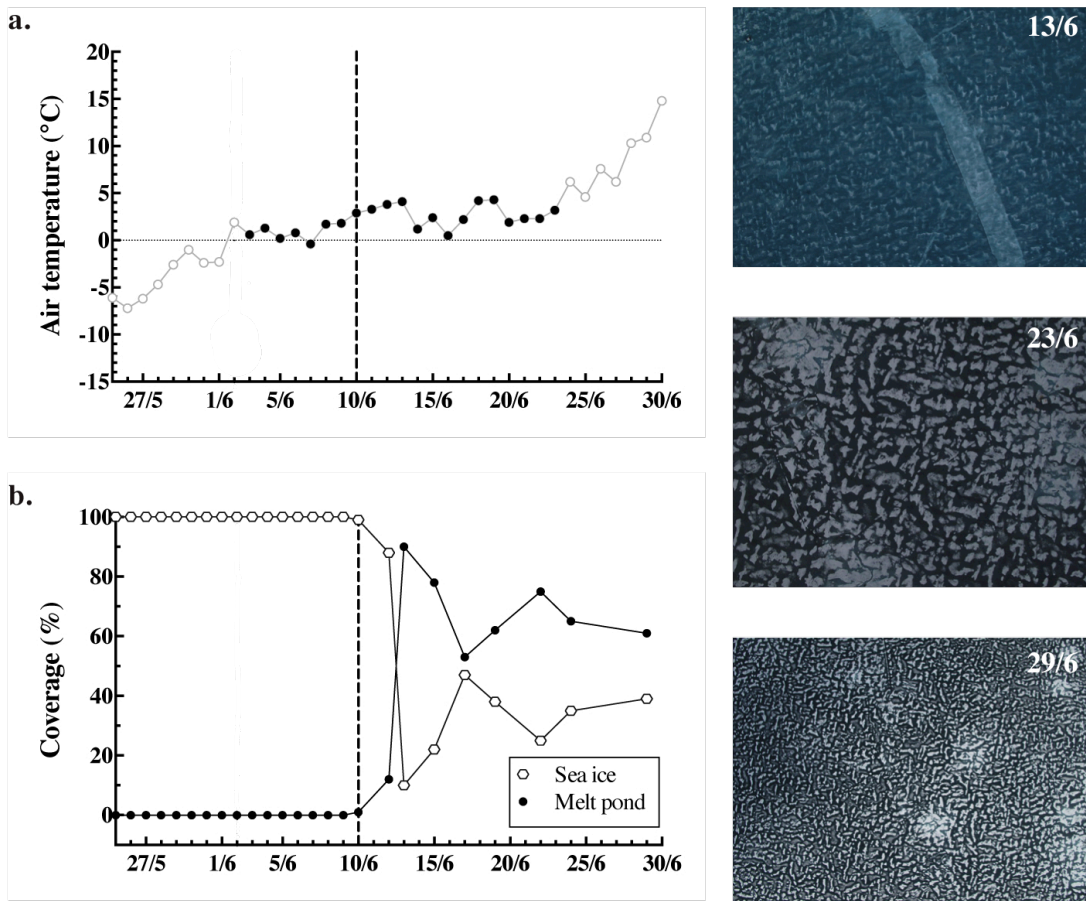
631 Figure 1: Location map of the sampling area in the Resolute Passage, Nunavut. The
632 sampling site was located between Sheringham Point and Griffith Island
633 (74.726°N, 95.576°W).



634

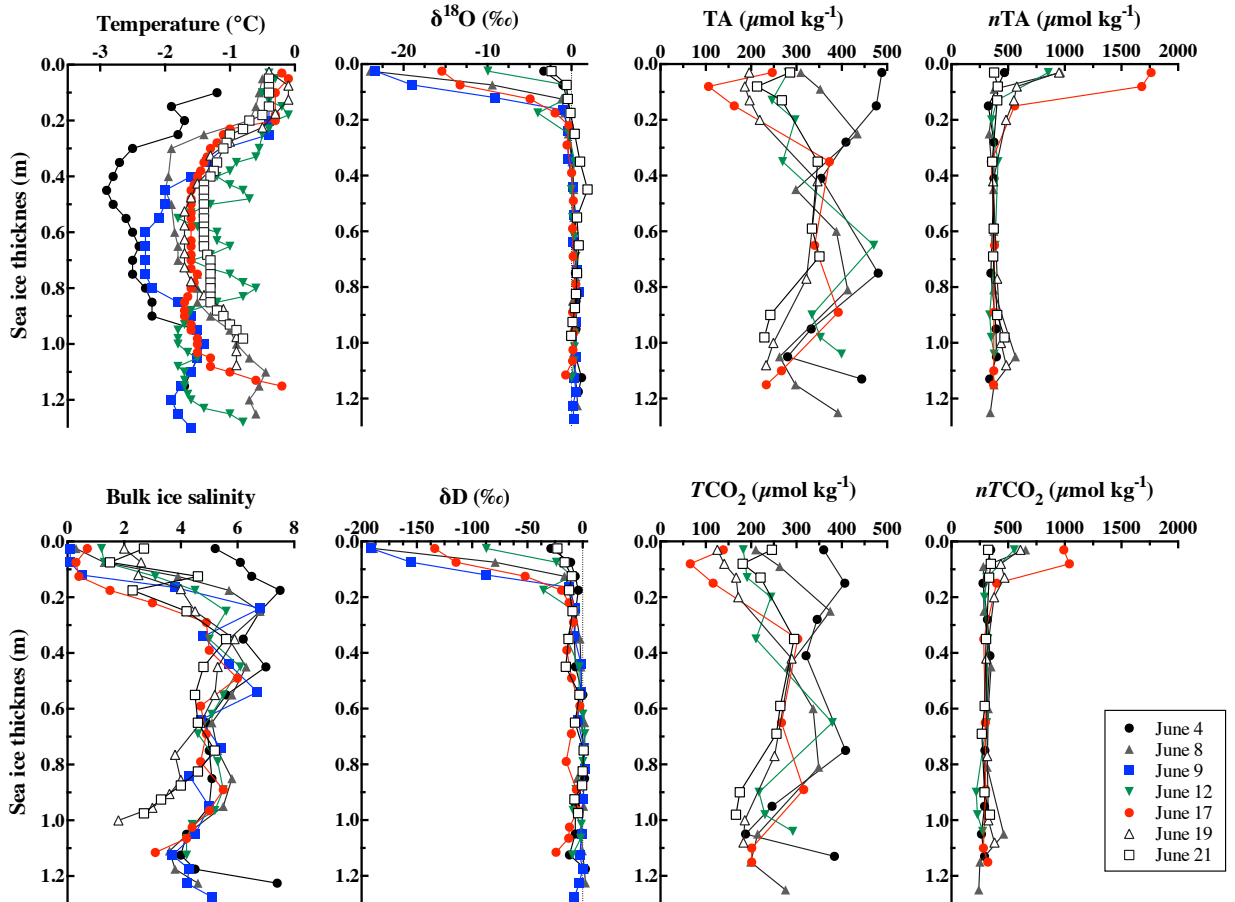
635

636 Figure 2: (a.) Evolution of the atmospheric temperature in Resolute from the end of
 637 May to the end of June 2012. The black dots represent the air temperature
 638 during our survey (from 3 to 23 June). (b.) Evolution of the melt ponds
 639 (black dots) and sea ice (white dots) fraction coverage at the sampling site.
 640 The bold dashed line on 10 June represents the initial formation of melt
 641 ponds at the surface of the ice cover. Aerial photo were taken over the field
 642 study site on 13 June (pond fraction = 0.9; width of the picture = 4472m),
 643 23 June (pond fraction = 0.65; width of the picture = 2212m), 29 June
 644 (pond fraction = 0.61; width of the picture = 4426m).
 645



646
 647

648 Figure 3: Sea ice profiles of temperature ($^{\circ}\text{C}$), salinity, isotopic composition of $\delta^{18}\text{O}$
 649 and δD (‰), TA_{ice} and $n\text{TA}_{\text{ice}}$ (in $\mu\text{mol kg}^{-1}$), TCO_2 and $n\text{TCO}_{2\text{ice}}$ (in $\mu\text{mol kg}^{-1}$).
 650
 651

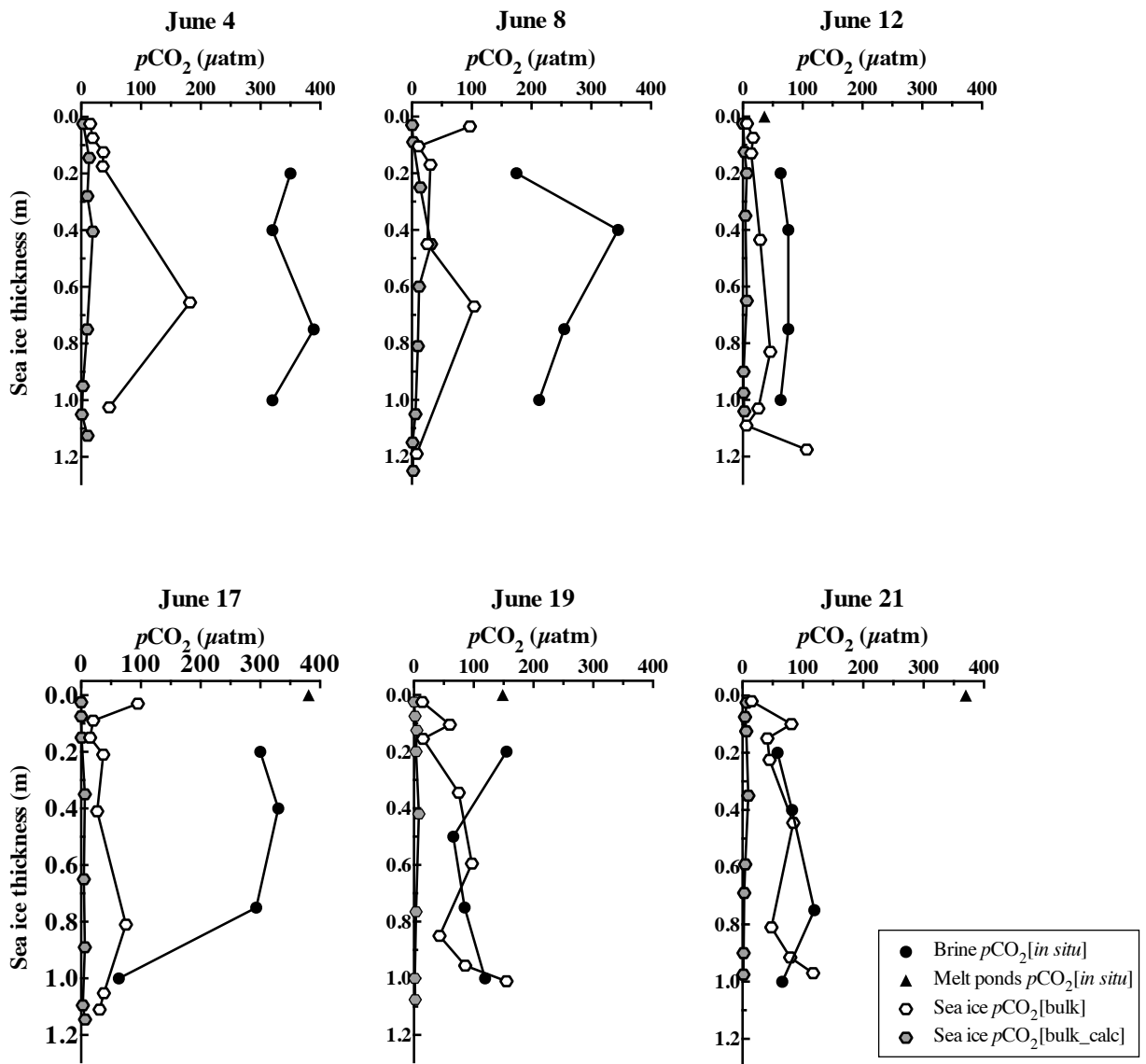


652

653

654 Figure 4: Sea ice profiles of $p\text{CO}_2$ (μatm) calculated from TA_{ice} and $\text{TCO}_{2\text{ice}}$ (grey
 655 diamonds) and *in situ* bulk sea ice $p\text{CO}_2$ (white diamonds). The *in situ* brine
 656 and melt ponds $p\text{CO}_2$ are also represented (back dots and triangle,
 657 respectively).

658

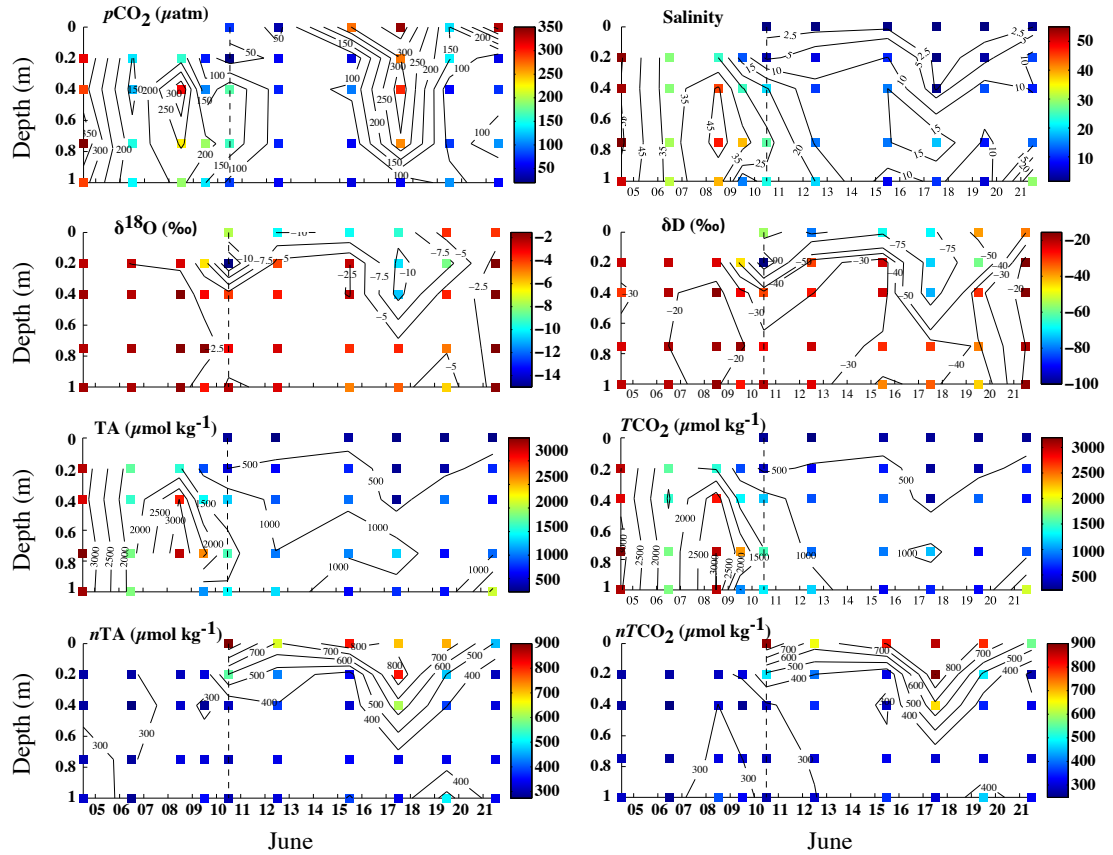


659

660

661

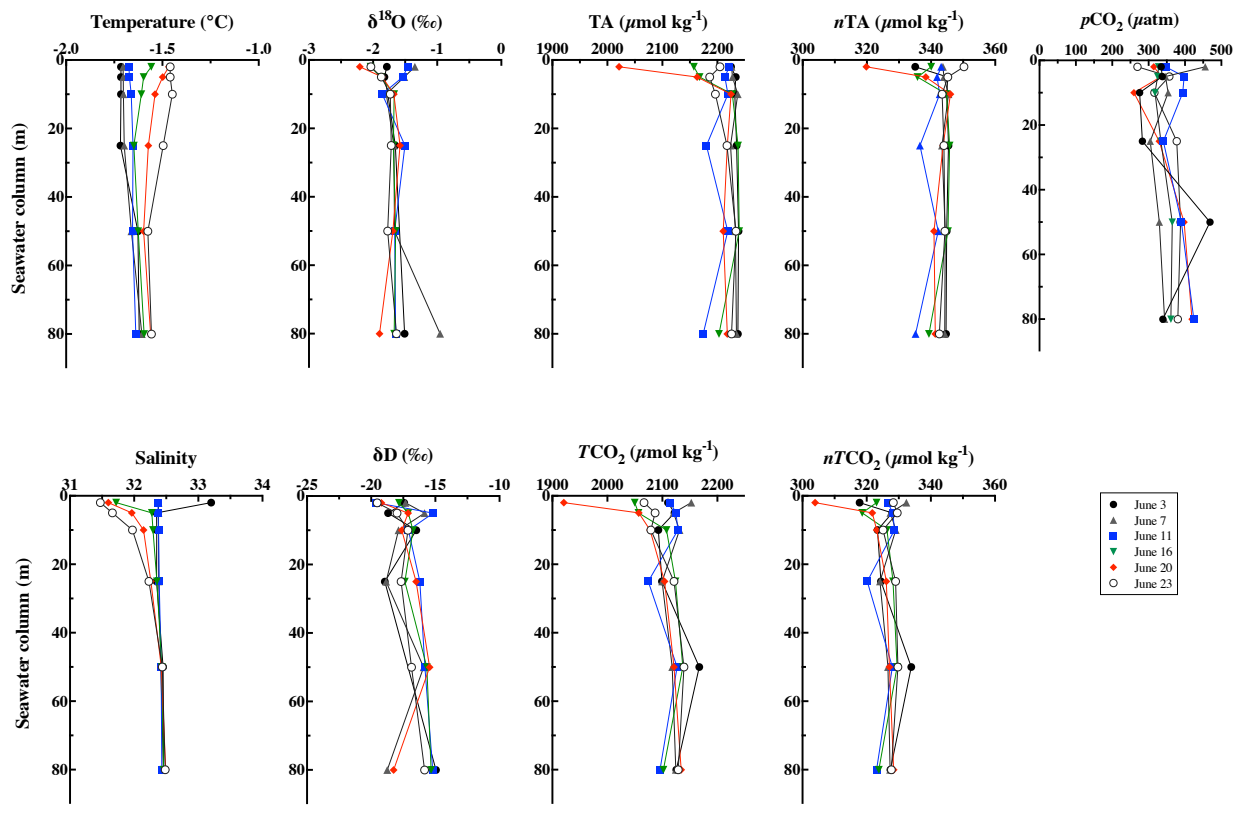
662 Figure 5: Profiles of *in situ* brine $p\text{CO}_2$ (in μatm), salinity, isotopic composition of $\delta^{18}\text{O}$
 663 and δD (‰), TA_{br} and $n\text{TA}_{\text{br}}$ (in $\mu\text{mol kg}^{-1}$), $\text{TCO}_{2\text{br}}$ and $n\text{TCO}_{2\text{br}}$ (in $\mu\text{mol kg}^{-1}$)
 664 1).



665
 666
 667
 668
 669

670 Figure 6: Water column profiles of temperature ($^{\circ}\text{C}$), salinity, isotopic composition of
 671 $\delta^{18}\text{O}$ and δD (‰), TA and $n\text{TA}$ (in $\mu\text{mol kg}^{-1}$), TCO_2 and $n\text{TCO}_2$ (in $\mu\text{mol kg}^{-1}$)
 672 and calculated $p\text{CO}_2$ (in μatm).

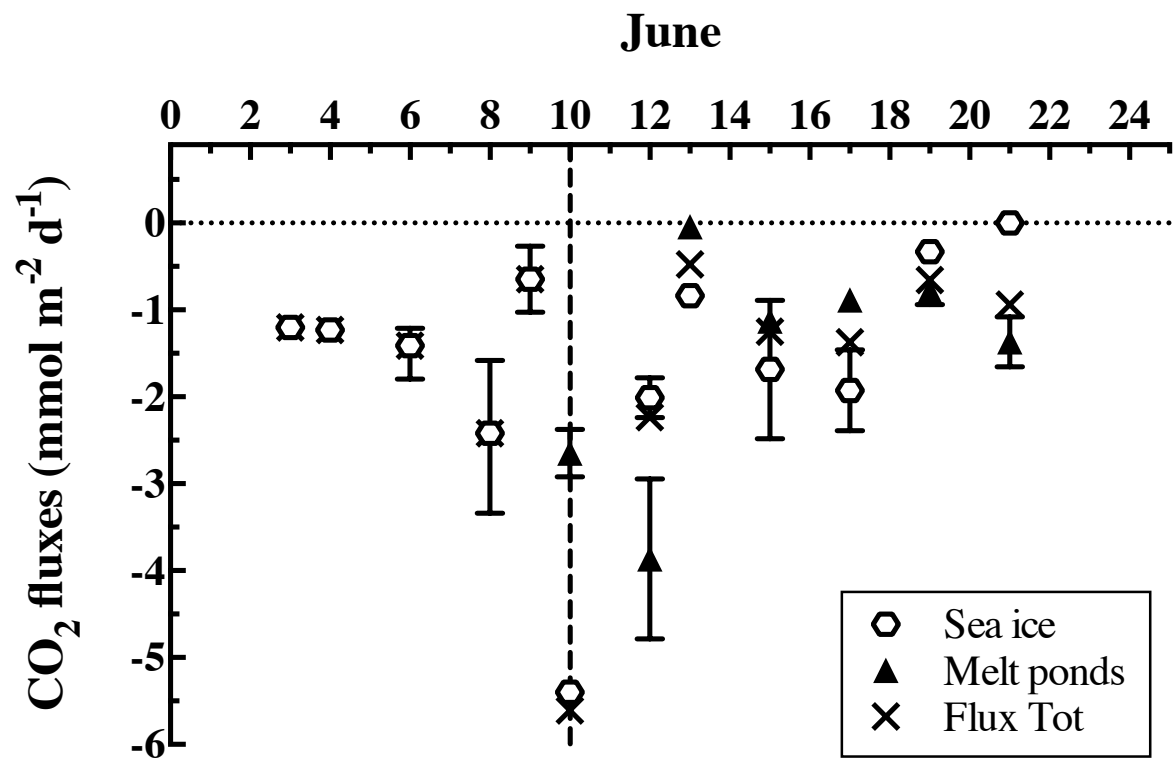
673
 674



675
 676
 677

678 Figure 7: CO₂ fluxes (in mmol m⁻² d⁻¹) measured over sea ice (white diamonds), melt
679 ponds (black triangle). The total fluxes are represented by the black cross.

680



681

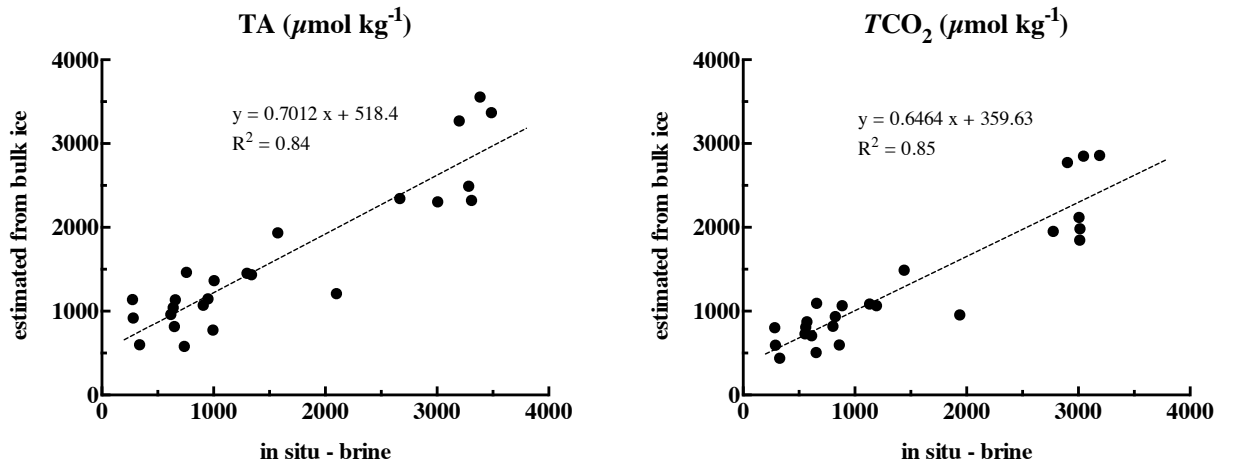
682

683

684

685 Figure 8: Comparison between brine TA and TCO_2 measured on brine collected using
686 the sackholes technique and the brine TA and TCO_2 estimated from TA_{ice} ,
687 TCO_{2ice} and the brine volume.

688

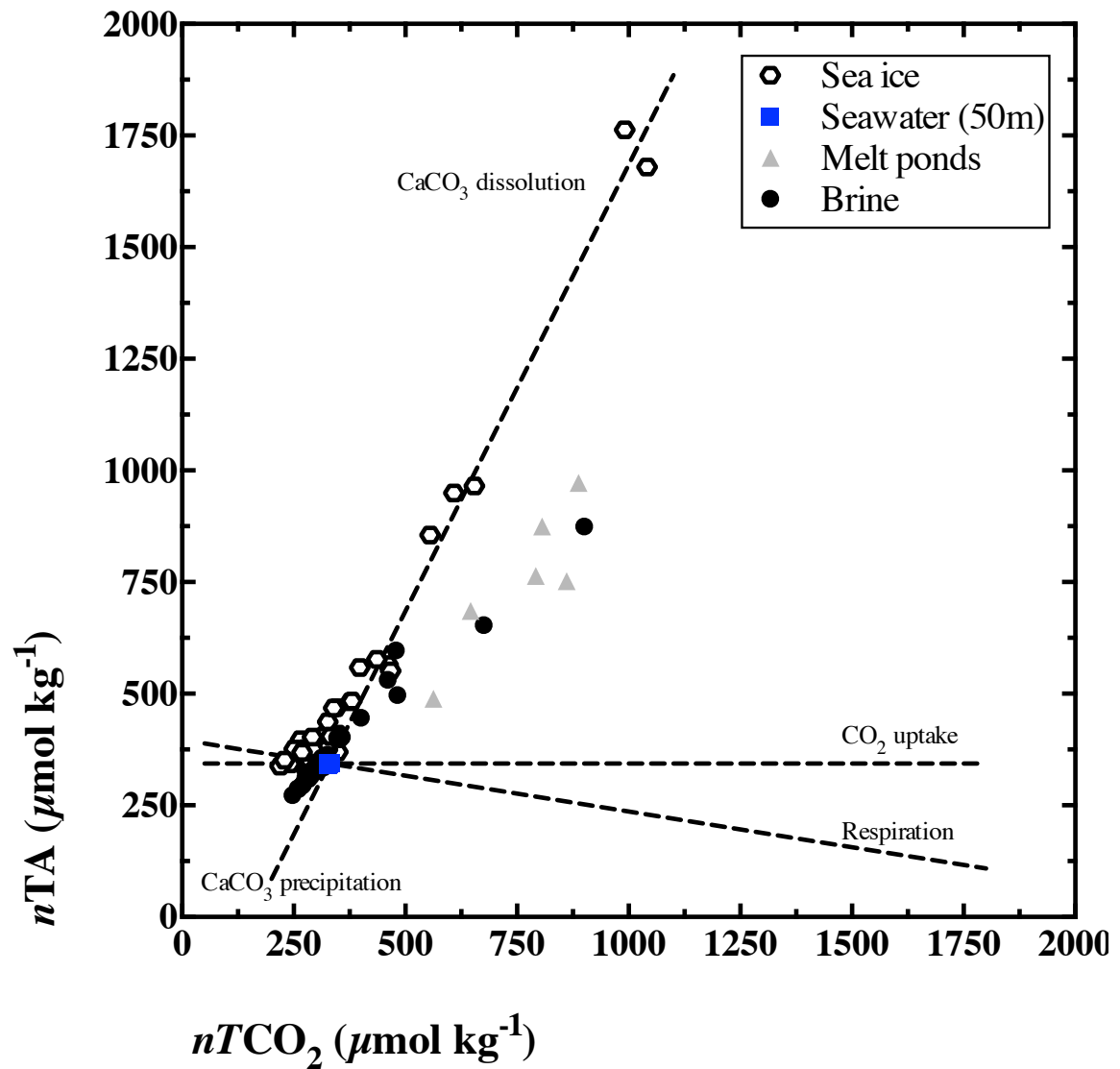


689

690

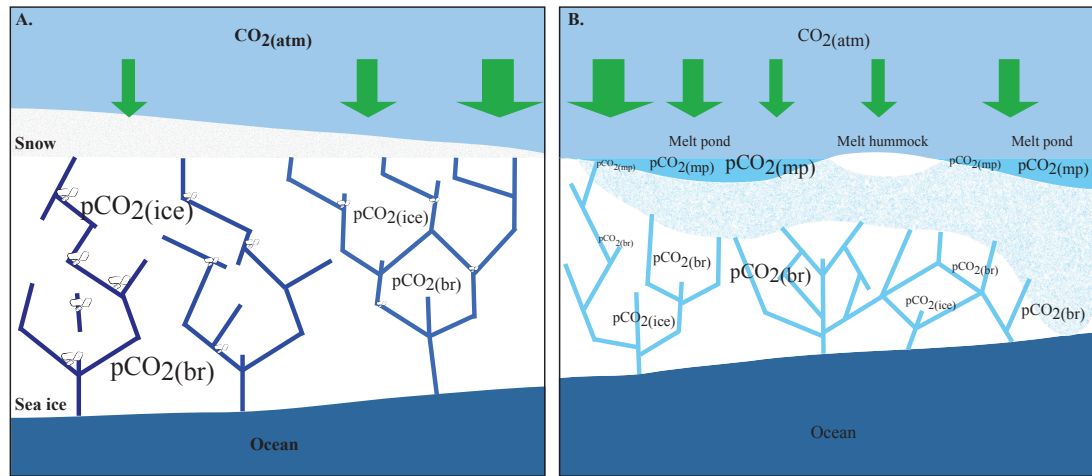
691

692 Figure 9: Relationship between the $n\text{TCO}_2$ and $n\text{TA}$ (in $\mu\text{mol kg}^{-1}$) in bulk sea ice
 693 (white diamonds), melt ponds (grey triangle) and brine samples (black
 694 dots). The different dashed lines represent the theoretical evolution of
 695 $n\text{TA}$: $n\text{TCO}_2$ ratio following the precipitation/dissolution of calcium
 696 carbonate, release/uptake of $\text{CO}_2(\text{g})$ and biological
 697 photosynthesis/respiration.



698
 699
 700

701 Figure 10: Schematic illustration of the inorganic carbon dynamics of melt pond-
702 covered first year sea ice. (a.) The increase of the ice temperature and the
703 decrease of the salinity, associated with the dissolution of ikaite crystals
704 promote the decrease of the bulk ice and brine $p\text{CO}_2$. (b.) Formation of melt
705 ponds at the surface of the ice and percolation of meltwater into the ice
706 matrix further decreases the $p\text{CO}_2$ with episodes of partial recovery, due to
707 surface exchanges with the atmosphere. The $p\text{CO}_2$ level is indicated by the size
708 of the writing. The intensity of the CO_2 uptake is indicated by the size
709 of the arrow.
710



711
712

713 9. Bibliography

- 714 Bates, N. R., and J. T. Mathis (2009), The Arctic Ocean marine carbon cycle: evaluation of air-
715 sea CO₂ exchanges, ocean acidification impacts and potential feedbacks, *Biogeosciences*,
716 6(11), 2433-2459.
- 717 Copin Montégut, C. (1988), A new formula for the effect of temperature on the partial
718 pressure of carbon dioxide in seawater, *Marine Chemistry*, 25, 29-37.
- 719 Cox, G. F. N., and W. F. Weeks (1974), Salinity variations in sea ice, *Journal of Glaciology*,
720 13(67), 109 - 120.
- 721 Cox, G. F. N., and W. F. Weeks (1983), Equations for determining the gas and brine volumes
722 in sea-ice samples, *Journal of Glaciology*, 29(102), 306 - 316.
- 723 Crabeck, O., B. Delille, D. N. Thomas, N. X. Geilfus, S. Rysgaard, and J. L. Tison (2014), CO₂
724 and CH₄ in sea ice from subarctic fjord, *Biogeosciences Discuss.*, 11, 4047-4083.
- 725 Dickson, A. G., and F. J. Millero (1987), A comparison of the equilibrium constants for the
726 dissociation of carbonic acid in seawater media, *Deep Sea Research*, I(34), 1733-1743.
- 727 Dieckmann, G. S., G. Nehrke, C. Uhlig, J. Göttlicher, S. Gerland, M. A. Granskog, and D. N.
728 Thomas (2010), Brief communication: Ikaite (CaCO₃·6H₂O) discovered in Arctic sea ice, *The*
729 *Cryosphere*, 4, 227-230.
- 730 Eicken, H., H. R. Krouse, D. Kadko, and D. K. Perovich (2002), Tracer studies of pathways and
731 rates of meltwater transport through Arctic summer sea ice, *Journal of Geophysical*
732 *Research-Oceans*, 107(C10), 8046.
- 733 Eicken, H., T. C. Grenfell, D. K. Perovich, J. A. Richter-Menge, and K. Frey (2004), Hydraulic
734 controls of summer Arctic pack ice albedo, *Journal of Geophysical Research-Oceans*, 109(C8),
735 13.
- 736 Fetterer, F., and N. Untersteiner (1998), Observations of melt ponds on Arctic sea ice,
737 *Journal of Geophysical Research-Oceans*, 103(C11), 24821-24835.
- 738 Frankignoulle, M. (1988), Field-Measurements of Air Sea CO₂ Exchange, *Limnology and*
739 *Oceanography*, 33(3), 313-322.
- 740 Freitag, J., and H. Eicken (2003), Meltwater circulation and permeability of Arctic summer
741 sea ice derived from hydrological field experiments, *Journal of Glaciology*, 49(166), 349-358.
- 742 Galindo, V., M. Levasseur, C. J. Mundy, M. Gosselin, J. É. Tremblay, M. Scarratt, Y. Gratton, T.
743 Papakiriakou, M. Poulin, and M. Lizotte (2014), Biological and physical processes
744 influencing sea ice, under-ice algae, and dimethylsulfoniopropionate during spring in the
745 Canadian Arctic Archipelago, *Journal of Geophysical Research: Oceans*, 119(6), 3746-3766.

- 746 Geilfus, N. X., B. Delille, V. Verbeke, and J. L. Tison (2012a), Towards a method for high
747 vertical resolution measurements of the partial pressure of CO₂ within bulk sea ice, *Journal*
748 *of Glaciology*, 58(208), 287-300.
- 749 Geilfus, N. X., G. Carnat, T. Papakyriakou, J. L. Tison, B. Else, H. Thomas, E. Shadwick, and B.
750 Delille (2012b), Dynamics of pCO₂ and related air-ice CO₂ fluxes in the Arctic coastal zone
751 (Amundsen Gulf, Beaufort Sea), *Journal of Geophysical Research-Oceans*, 117(C00G10).
- 752 Geilfus, N. X., G. Carnat, G. S. Dieckmann, N. Halden, G. Nehrke, T. Papakyriakou, J. L. Tison,
753 and B. Delille (2013a), First estimates of the contribution of CaCO₃ precipitation to the
754 release of CO₂ to the atmosphere during young sea ice growth, *Journal of Geophysical*
755 *Research*, 118.
- 756 Geilfus, N. X., R. J. Galley, M. Cooper, N. Halden, A. Hare, F. Wang, D. H. Sjøgaard, and S.
757 Rysgaard (2013b), Gypsum crystals observed in experimental and natural sea ice,
758 *Geophysical Research Letters*, 2013GL058479.
- 759 Gleitz, M., M. R. vd Loeff, D. N. Thomas, G. S. Dieckmann, and F. J. Millero (1995), Comparison
760 of summer and winter inorganic carbon, oxygen and nutrient concentrations in Antarctic
761 sea ice brine, *Marine Chemistry*, 51(2), 81-91.
- 762 Glud, R. N., S. Rysgaard, G. Turner, D. F. McGinnis, and R. J. G. Leakey (2014), Biological- and
763 physical-induced oxygen dynamics in melting sea ice of the Fram Strait, *Limnology and*
764 *Oceanography*, 59(4), 1097-1111.
- 765 Hansen, J. W., B. Thamdrup, and B. B. Jørgensen (2000), Anoxic incubation of sediment in
766 gas-tight plastic bags: a method for biogeochemical processes studies, *Marine Ecology-*
767 *Progress Series*, 208, 273-282.
- 768 Hanson, A. M. (1965), Studies of the mass budget of arctic pack-ice floes, *Journal of*
769 *Glaciology*, 5(41), 701-709.
- 770 Haraldsson, C., L. G. Anderson, M. Hasselov, S. Hulth, and K. Olsson (1997), Rapid, high-
771 precision potentiometric titration of alkalinity in ocean and sediment pore waters, *Deep sea*
772 *Research I*, 44(12), 2031-2044.
- 773 Landy, J. C., J. K. Ehn, M. Shields, and D. G. Barber (2014), Surface and melt pond evolution
774 on landfast first-year sea ice in the Canadian Arctic Archipelago, *Journal of Geophysical*
775 *Research: Oceans*, 119(5), 3054-3075.
- 776 Lazar, B., and Y. Loya (1991), Bioerosion of coral reefs - A chemical approach, *Limnology*
777 *and Oceanography*, 36(2), 377-383.
- 778 Leppäranta, M., and T. Manninen (1988), The brine and gas content of sea ice with attention
779 to low salinities and high temperatures *Rep.*, Helsinki.

780 Mehrbach, C., C. H. Culberson, J. E. Hawley, and R. M. Pytkowicz (1973), Measurements of
781 the apparent dissociation constants of carbonic acid in seawater at atmospheric pressure,
782 *Limnology and Oceanography*, 18, 897-907.

783 Miller, L. A., G. Carnat, B. G. T. Else, N. Sutherland, and T. N. Papakyriakou (2011), Carbonate
784 system evolution at the Arctic Ocean surface during autumn freeze-up, *Journal of*
785 *Geophysical Research*, 111(C00G04).

786 Mundy, C. J., et al. (2011), Characteristics of two distinct high-light acclimated algal
787 communities during advanced stages of sea ice melt, *Polar Biol.*, 34(12), 1869-1886.

788 Nomura, D., H. Eicken, R. Gradinger, and K. Shirasawa (2010a), Rapid physically driven
789 inversion of the air-sea ice CO₂ flux in the seasonal landfast ice off Barrow, Alaska after
790 onset surface melt, *Continental Shelf Research*, 30(19), 1998-2004.

791 Nomura, D., H. Yoshikawa-Inoue, T. Toyota, and K. Shirasawa (2010b), Effects of snow,
792 snow-melting and re-freezing processes on air-sea ice CO₂ flux, *Journal of Glaciology*,
793 56(196), 262-270.

794 Nomura, D., M. A. Granskog, P. Assmy, D. Simizu, and G. Hashida (2013), Arctic and Antarctic
795 sea ice acts as a sink for atmospheric CO₂ during periods of snowmelt and surface flooding,
796 *Journal of Geophysical Research: Oceans*, 6511-6524.

797 Papadimitriou, S., H. Kennedy, L. Norman, D. P. Kennedy, G. S. Dieckmann, and D. N. Thomas
798 (2012), The effect of biological activity, CaCO₃ mineral dynamics, and CO₂ degassing in the
799 inorganic carbon cycle in sea ice and late winter-early spring in the Weddell Sea, Antarctica,
800 *Journal of Geophysical Research*, 117(C08011).

801 Papakyriakou, T., and L. Miller (2011), Springtime CO₂ exchange over seasonal sea ice in the
802 Canadian Arctic Archipelago, *Annals of Glaciology*, 52(57).

803 Parmentier, F.-J. W., T. R. Christensen, L. L. Sørensen, S. Rysgaard, A. D. McGuire, P. A. Miller,
804 and D. A. Walker (2013), The impact of lower sea-ice extent on Arctic greenhouse-gas
805 exchange, *Nature climate change*, 195-202.

806 Perovich, D. K., W. B. Tucker, and K. A. Ligett (2002), Aerial observations of the evolution of
807 ice surface conditions during summer, *Journal of Geophysical Research-Oceans*, 107(C10),
808 8048.

809 Perovich, D. K., K. F. Jones, B. Light, H. Eicken, T. Markus, J. Stroeve, and R. Lindsay (2011),
810 Solar partitioning in a changing Arctic sea-ice cover, *Annals of Glaciology*, 52(57), 192-196.

811 Polashenski, C., D. Perovich, and Z. Courville (2012), The mechanisms of sea ice melt pond
812 formation and evolution, *Journal of Geophysical Research: Oceans*, 117(C1), C01001.

- 813 Rösel, A., and L. Kaleschke (2012), Exceptional melt pond occurrence in the years 2007 and
814 2011 on the Arctic sea ice revealed from MODIS satellite data, *Journal of Geophysical*
815 *Research-Oceans*, 117.
- 816 Rysgaard, S., R. N. Glud, M. K. Sejr, J. Bendtsen, and P. B. Christensen (2007), Inorganic
817 carbon transport during sea ice growth and decay: A carbon pump in polar seas, *Journal of*
818 *Geophysical Research-Oceans*, 112(C3).
- 819 Rysgaard, S., R. N. Glud, K. Lennert, M. Cooper, N. Halden, R. J. G. Leakey, F. C. Hawthorne,
820 and D. Barber (2012a), Ikaite crystals in melting sea ice – implications for pCO₂ and pH
821 levels in Arctic surface waters, *The Cryosphere*, 6, 1-8.
- 822 Rysgaard, S., J. Bendtsen, B. Delille, G. S. Dieckmann, R. N. Glud, H. Kennedy, J. Mortensen, S.
823 Papadimitriou, D. N. Thomas, and J. L. Tison (2011), Sea ice contribution to the air-sea
824 CO₂ exchange in the Arctic and Southern Oceans, *Tellus Series B-Chemical and Physical*
825 *Meteorology*, 63(5), 823-830.
- 826 Rysgaard, S., J. Mortensen, T. Juul-Pedersen, L. L. Sørensen, K. Lennert, D. H. Sjøgaard, K. E.
827 Arendt, M. E. Blicher, M. K. Sejr, and J. Bendtsen (2012b), High air-sea CO₂ uptake rates in
828 nearshore and shelf areas of Southern Greenland: Temporal and spatial variability, *Marine*
829 *Chemistry*, 128-129, 26-33.
- 830 Rysgaard, S., et al. (2014), Temporal dynamics of ikaite in experimental sea ice, *The*
831 *Cryosphere*, 8(4), 1469-1478.
- 832 Rysgaard, S., et al. (2013), Ikaite crystal distribution in winter sea ice and implications for
833 CO₂ system dynamics, *The Cryosphere*, 7(2), 707-718.
- 834 Semiletov, I. P., A. Makshtas, S. I. Akasofu, and E. L. Andreas (2004), Atmospheric CO₂
835 balance: The role of Arctic sea ice, *Geophysical Research Letters*, 31(5).
- 836 Sjøgaard, D. H., D. N. Thomas, S. Rysgaard, L. Norman, H. Kaartokallio, T. Juul-Pedersen, R. N.
837 Glud, and N. X. Geilfus (2013), The relative contributions of biological and abiotic processes
838 to the carbon dynamics in subarctic sea ice, *Polar Biol.*
- 839 Takahashi, T., et al. (2009), Climatological mean and decadal change in surface ocean pCO₂,
840 and net sea-air CO₂ flux over the global oceans, *Deep-Sea Research Part II-Topical Studies in*
841 *Oceanography*, 56(8-10), 554-577.
- 842 Taylor, P. D., and D. L. Feltham (2004), A model of melt pond evolution on sea ice, *Journal of*
843 *Geophysical Research-Oceans*, 109(C12).
- 844 Untersteiner, N. (1968), Natural desalination and equilibrium salinity profile of perennial
845 sea ice, *Journal of Geophysical Research*, 73(4), 1251 - 1257.
- 846 Weeks, W. F. (Ed.) (2010), *On sea ice*, 664 pp., Fairbanks, Alaska.

- 847 Zeebe, R. E., and D. Wolf-Gladrow (2001), *CO₂ in seawater: Equilibrium, Kinetics, Isotopes*,
848 Elsevier.
- 849 Zeebe, R. E., H. Eicken, D. H. Robinson, D. WolfGladrow, and G. S. Dieckmann (1996),
850 Modeling the heating and melting of sea ice through light absorption by microalgae, *Journal*
851 *of Geophysical Research-Oceans*, 101(C1), 1163-1181.
- 852 Zhou, J. Y., B. Delille, H. Eicken, M. Vancoppenolle, F. Brabant, G. Carnat, N. X. Geilfus, T.
853 Papakyriakou, B. Heinesch, and J. L. Tison (2013), Physical and biogeochemical properties
854 in landfast sea ice (Barrow, Alaska): Insights on brine and gas dynamics across seasons,
855 *Journal of Geophysical Research-Oceans*, 118(6), 3172-3189.
856